JJMIE

Volume 18, Number 2, June. 2024
ISSN 1995-6665
Pages 311- 326
https://doi.org/10.59038/jjmie/180205
Editor-in-Chief: Prof. Ali M. Jawarneh

Jordan Journal of Mechanical and Industrial Engineering

Investigating Spot Weld Fatigue Failure with Experimental and Finite Element Analysis Methods

Marwah Sabah Fakhri[1,2], Ahmed Al-Mukhtar[3,4*], Ibtihal A. Mahmood[2]

[1]Ministry of Higher Education and Scientific Research-Baghdad, Iraq
[2]University of Technology-Iraq, Mechanical Engineering Department, Baghdad, Iraq
[3]College of Engineering, Al-Hussain University College, Iraq
[4]Institute of Structural Mechanics, Bauhaus-Universität Weimar, Germany

Received 29 Feb 2024 *Accepted 13 Apr 2024*

Abstract

Resistance spot welding (RSW) is the most commonly used method for joining sheet metals structures in the automotive industry. The cyclic loading conditions on RSW joints can lead to fatigue failure, hence, affecting their reliability and durability. The comprehension of the fatigue strength for the RSW is very critical, especially for the dissimilar RSW joints. This study presents analyses to characterize the fatigue behavior of these joints. Therefore, the crack propagation, and fatigue life under specific loading conditions have been studied. The fatigue strength of similar aluminum Al-1050, and dissimilar copper with aluminum Cu-Al RSW joints was examined experimentally and numerically. The lap-sheet materials were spot welded using optimum welding parameters to ensure a consistent range for the produced weld nugget. In this work, the experimental test rig has been designed and established to have an axial fatigue load. The high cycle fatigue tests were performed, and the P-N curves were obtained. The work was analyzed numerically using finite element (FE) analysis, in conjunction with experimental results. Aluminum sheet joint has the highest fatigue limit as compared to dissimilar Cu-Al joints. The crack growth rate of the similar RSW joint is slower than those of dissimilar joints because it has higher stress intensity factor (SIF). The coefficients of the Paris' constants, C and m, have been determined.

Keywords: Crack Propagation; Fatigue Crack; Fatigue Life; Fracture; Resistance Spot Welding.

1. Introduction

The RSW is a type of resistance welding where the heat required for fusion is generated by the resistance to electric current flow between the two or more metal surfaces [1]. This process involves applying pressure, hence, passing a high electric current for a short time. The two sheets are held together by electrodes. The heat is generated at the interface between the work pieces. Hence, it forms a strong metallurgical bond. Copper electrodes are typically used to conduct the current and apply pressure evenly across the joint area [2], [3].

The fatigue crack begins at the interior surface of the welded sheets in the heat-affected zone (HAZ) [4], [5]. Therefore, it is very important to know the crack growth rate in the spot-welded member, to determine the durability of the spot weld before rupture [6]. Mechanical fracture is the most common type of failure that must be taken into consideration in structural or mechanical machines and applications [7], [8], [9]. The vast majority of mechanical applications, including aircraft and automobiles, are subjected to fatigue loads [10], [11]. However, composite materials are widely used for such applications due to their weight and strength properties [12], [13]. Joining composite materials in sheet form is not possible using high-temperature methods such as spot welding. Assessment of optimum spot-weld performance during the cyclic loading is more difficult than during the static loading [14]. In fatigue, repetitive (cyclic) loading can initiate and advance a crack at stresses below the design strength [15]. Spot welding failure may severely affect any mechanical assembly, resulting in significant damage. Therefore, spot welds must be designed to be strong to ensure proper functioning [16]. Variations in the spot-weld region microstructure, welding parameters, and many other factors make it very difficult to understand the failure associated with the fatigue of RSW sheets [17], [18]. At the weld nuggets, three distinct zones with different microstructures are produced, fusion zone (FZ) heat-affected zone (HAZ), and the base metal (BM) [19], [20].

The effects of the weld parameters (welding time, welding current, and electrode force) and post-heating treatments effects on the weld size, residual stresses, and the fatigue life of similar weld joints have been investigated [21], [22], [23], [24], [25], [26], [27], [28]. However, no studies have investigated either the fracture behavior of dissimilar spot welds in Al-Cu joints or the FE simulation of such joints.

* Corresponding author e-mail: almukhtar@structuralintegrity.eu.

In this study, copper and aluminum 1050 sheet materials were spot welded to form lap joints for conducting tensile and fatigue tests. Consequently, an experimental test rig was designed and built to measure the fatigue life and crack propagation. Additionally, a numerical finite element (FE) model was developed and its results were benchmarked. The applied fatigue load and number of cycles were presented through P-N curves. The fatigue life material coefficients, c and m, have been calculated for similar and dissimilar joints. The crack growth rate curve was investigated and compared to the data given in the literature.

2. Methodology

2.1. Experimental Work

2.1.1. Materials

The commercial T2 Cu and Al-1050 sheets were used. The current metals have a traditional use for structural and electrical requirements [29]. The chemical analysis was conducted for Al, and Cu, respectively; see Tables 1, and 2. Additionally, the mechanical properties of base metals were determined through tensile testing and microstructural analysis (see Fig. 1).

The specimens for the as-received metals are prepared in accordance with the standard specifications ASTM E8/E8M−13a, see Ref. [29]. The specimens were formed using a CNC machine. Samples are cut along the rolling directions to calculate the ultimate stress; see Fig. 2. It is noteworthy that the specimens cut in the direction of rolling exhibited a slightly higher tensile strength owing to the elongated grain structure, which contributes to enhanced strength [30]. Nevertheless, the differences in the weld strength are small because the fractures usually occur in the weld area or inside the HAZ.

A tensile test for specimens was carried out to determine the mechanical properties of each material (yield strength σ_y, ultimate tensile strength σ_{uts}, modulus of elasticity E, and elongation); see Table 3. In addition, some other metals, which were collected in Table 3, were used to validate the FE model. Three samples were taken for each material, Cu and Al, to obtain the most accurate results, as shown in, see Fig. 3. The tensile test was carried out using a universal testing machine with a speed rate of 1 mm/min [31]. The average values of three specimens were taken. These results were utilized as input data for simulating resistance spot welding (RSW) in Abaqus.

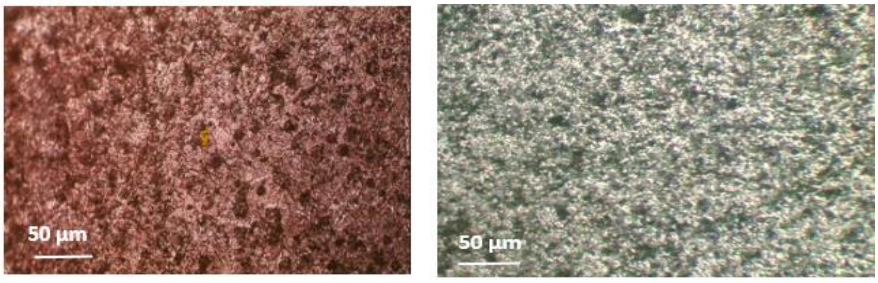

(a) (b)

Figure 1. Microstructure of base metal (5x): (a) Cu; (b) Al

Table1. Chemical compositions of Al-1050

	Element (wt. %)							
Material	Si	Fe	Cu	Mn	Mg	Zn	Ti	AL
Al-1050	0.047	0.4	0.048	0.0033	0.0012	0.0027	0.021	99.5

Table 2. Chemical compositions of T_2 grade pure copper

	Element (wt. %)									
Material	**Zn**	**Pb**	**P**	**Mn**	**Fe**	**Ni**	**Si**	**Mg**	**AL**	**Cu**
T_2 Cu	0.003	0.0003	0.0008	0.0004	0.007	0.0002	0.0008	0.0001	0.002	≤100

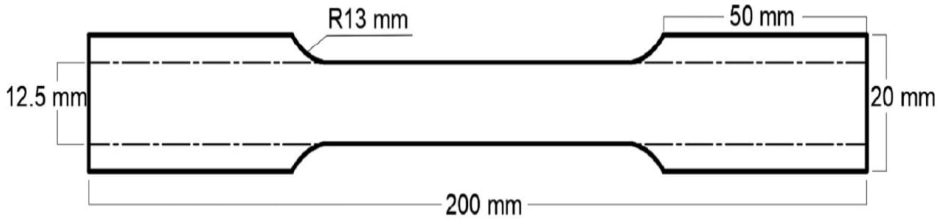

Figure 2. Tensile specimen and dimensions

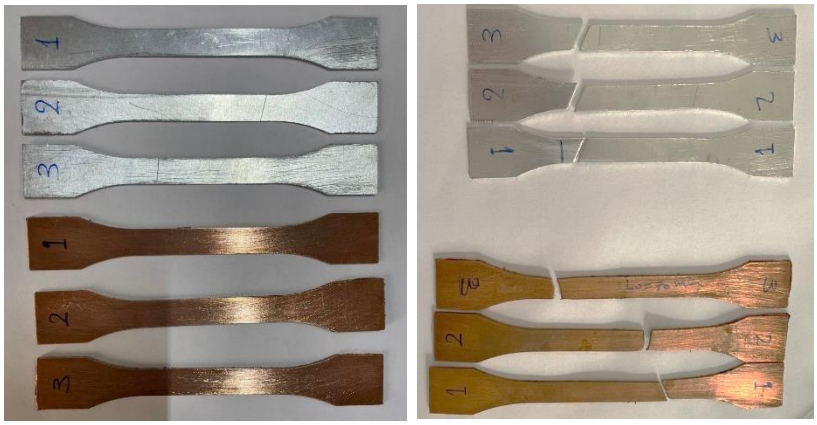

a)

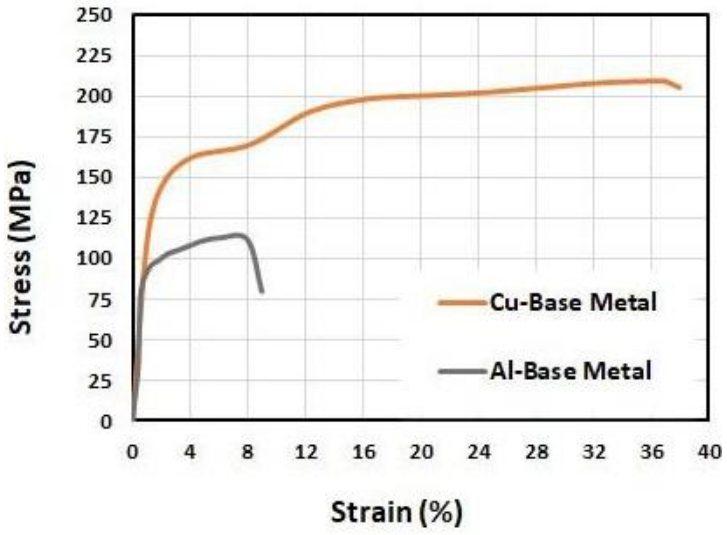

b)

Figure 3. a) Tensile test samples of Cu, and Al; b) Stress-strain curve of base metals

Table 3. Mechanical properties of some materials

	Mechanical Properties			
Metals	**σ_y (MPa)**	**σ_{uts} (MPa)**	**E (GPa)**	**El. %**
Cu	144	209	129	34
Al-1050	80	112	67	7.8
Al-6061 [32]	279	310	79.8	8
Al-5052 [33]	193	228	70.3	26
Steel [34]	370	758	190- 210	4-31

For the numerical model, some other properties are required, such as the physical properties; see Table 4. These properties serve as crucial input parameters for the ABAQUS simulation, enabling precise modeling and analysis of the welded materials in the study.

2.1.2. RSW Processes

The sheet materials were cut into 100 mm × 25 mm according to AWS C1.1 standard [39]. The RSW is a solid-state joining method that involves heating the connecting surfaces of the sheet metal components; see Fig. 4. As the heat and temperature increase, the resistance to current at the contact surfaces will increase. Hence, localized nuggets occur at the interface between the two surfaces as the metal surfaces start to melt [40]. To ensure proper surface contact, pressure is also applied to the copper electrodes. After that, the current is cut off, but the pressure, still exerted on the surfaces, guarantees that the metals will cool and solidify [39].

Table 4: Physical properties of some materials [35]

Properties	Unit	Al 1050 [36]	Cu [35]	Al 6061 [37]	Al 5052 [38]	Steel[34]
Density	g/cm^3	2.70	8.94	2.7	2.8	7.8
Resistance	(Ωmm^2 /m) x10^2	2.66	1.68	3.2	3.5	1.89
Thermal Conductivity	cal/cm^2 /cm°Cs	0.52	0.92	0.5	0.52	0.11
Thermal Coef. of Linear Expansion	(mm/mm°C) x10^{-6}	24.00	16.70	22.00	23.00	25.3
Specific Heat Capacity	J/kg°C	902	385	905	908	431
Melting Temperature	°C	660	1083	571	588	1516
Poisson Ratio	--	0.31	0.33	0.33	0.33	0.3

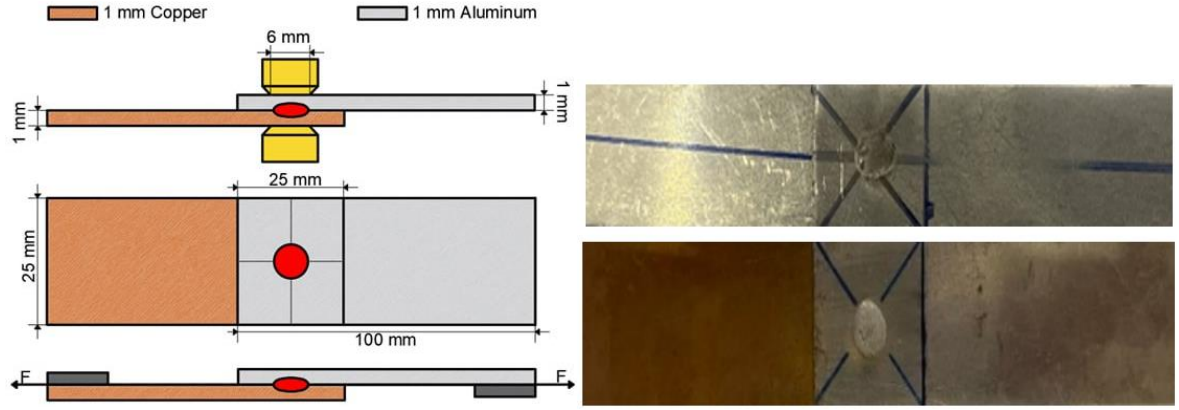

Figure 4. RSW process and specimen dimensions

2.1.3. Welding Parameters

Lap-shear specimens can be made from similar or dissimilar sheet combinations, depending on the application and research objectives. This work aimed to examine the crack propagation and fatigue life of RSW similar and dissimilar joints. Hence, the optimum weld joints were welded according to the best weld parameters for such metals and thicknesses. In the case of similar spot metal welding, it was simple to specify the welding parameters in accordance with the AWS C1.1 M/C1 standard and literature; see Ref. [39]. Table 5 presents the resistance spot welding (RSW) parameters utilized for Al-Al spot welds with a thickness of 1 mm.

Table 5. RSW parameters for Al-Al spot weld for 1 mm thickness

Joint	Current (A.)	Electrode Force (N)	Weld time (S)
Al-Al [41]	14000	7000	0.8

In the case of dissimilar Al-Cu spot weld joints, the optimum welding parameters were determined. These optimal parameters were determined after welding numerous samples, conducting a tensile test, and selecting the sample with the highest tensile strength. The strength was calculated as the average of readings from at least three specimens. This process was validated using the statistical Taguchi approach [42], [43]. It is one of the greatest techniques for optimization, because it reduces the number of trials by organizing the tests into an orthogonal array and choosing the most useful parameters (current, time, and pressure) [44], [45]. This method is utilized to examine the impact of each welding parameter on the tensile force separately. As a result, it was found that the energy produced during the welding depends on the electrical current, the time the current flows, and contact resistance. Since the type and shape of the electrode have an influence on pressure [46]. Figure 5 shows the major effects of these variables on the response variable (tensile force).

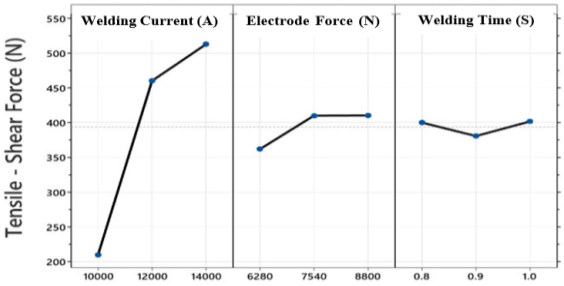

Figure 5. RSW parameters as per the Taguchi Technique

The optimum RSW parameters that were calculated at the maximum tensile shear force are listed in Table 6. Hence, they were used in this instigation for dissimilar joints.

Table 6. RSW parameters for dissimilar joint Al-Cu

Joint	Current (Amp.)	Electrode Force (N)	Welding time (sec)
Al-Cu	14000	8800	1

2.1.4. Tensile Shear Test

The spot weld specimens were prepared for the tensile-shear test according to AWS C1.1 [39]. Two sheets, 100 mm long and 25 mm wide, of a thickness of 1 mm and overlapping 25 mm, have been welded with a single spot-welding nugget; see Fig. 6. The same dimensions are used for both similar and dissimilar joints.

The RSW specimens were gripped with alignment tabs of a thickness equal to that of the specimens to ensure that the tensile force was applied to the weld spot and to avoid bending [47]. The average values have been taken from different measurements.

To validate the current experiment and FE models, the tensile shear results have been compared to the literature. Hence, the tensile test reveals whether the weld satisfies the necessary standards for strength and ductility. A universal testing equipment with a 1 mm/min deformation rate was used for the tensile-shear testing.

2.1.5. Fatigue Test

The axial fatigue test was carried out on a welded sample using a specially designed fatigue rig with a 10 Hz loading frequency and a 2.5 kN maximum load capacity. The mechanical spring that was connected to load cell Type-S was used to apply the axial fatigue load; see Fig. 7.

The load cell is an essential component of the apparatus that measures the force applied to the specimen. The HX711 is a signal amplifier that can be used to read the output of the load cell and convert it into a digital signal that can be read by a microcontroller Arduino Uno 12. The signal from the load cell passes through an amplifier and then goes to an Arduino to measure the fatigue load from the computer. The data received from the apparatus to the computer is represented by the load profile with the number of cycles; see Fig. 8.

First, the maximum applied load was calibrated by using the flat specimen (not welded) with the same dimension as the RSW sample, to determine required initial force.

The same SW specimen dimensions that were used in the tensile-shear test (see Fig. 4) were used in the fatigue test. In the fatigue test, both sides of the specimen were pierced for fixation purposes using a locally designed device; see Fig. 9.

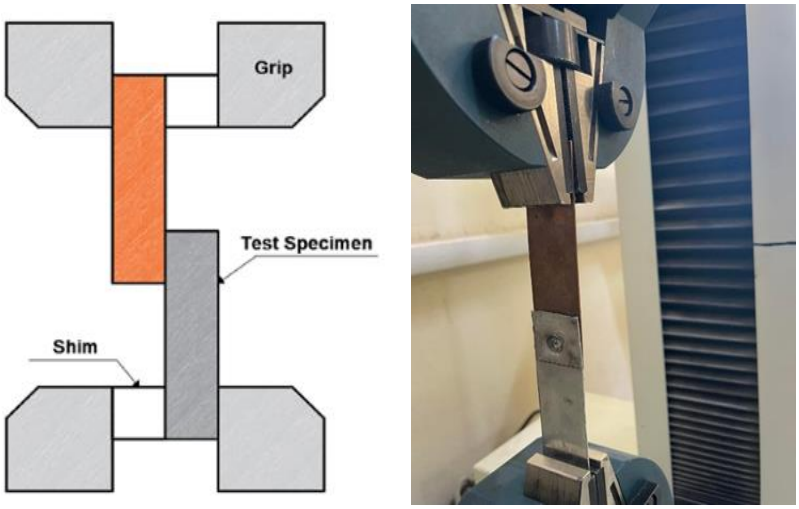

Figure 6. Tensile shear test; a) specimens with alignments tab, b) specimens gripped

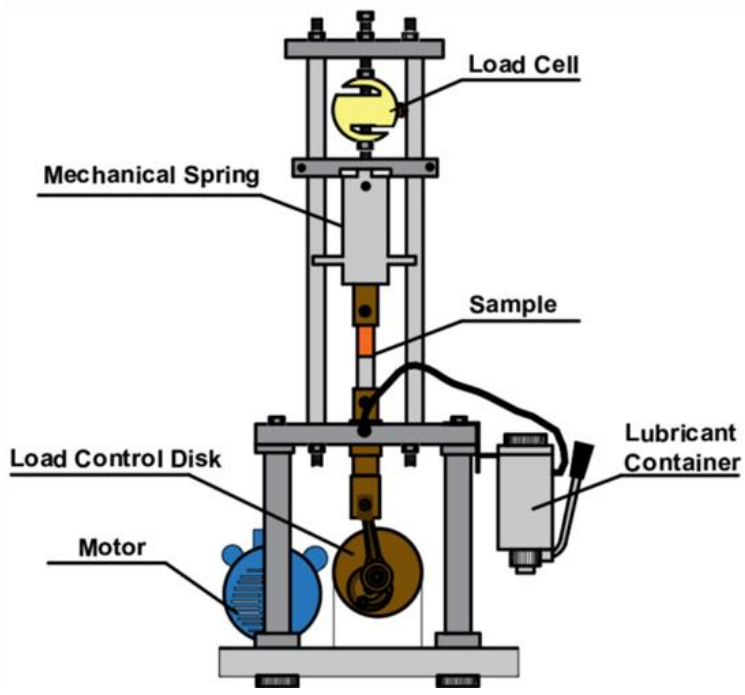

Figure 7. Schematics of axial fatigue rig

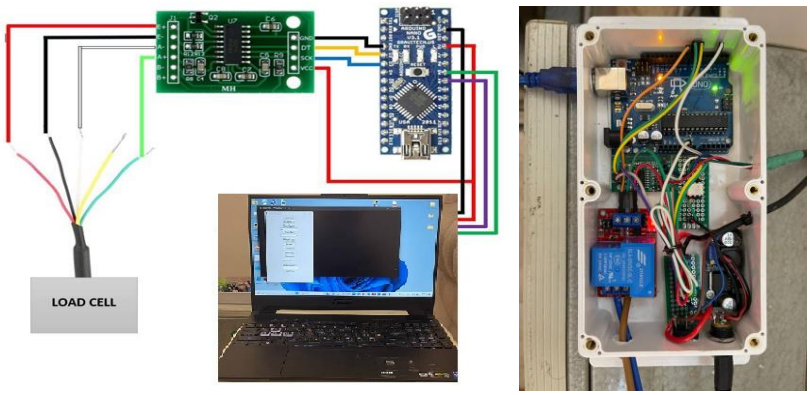

Figure 8. Load cell, amplifier, Arduino, and computer connection to the fatigue device

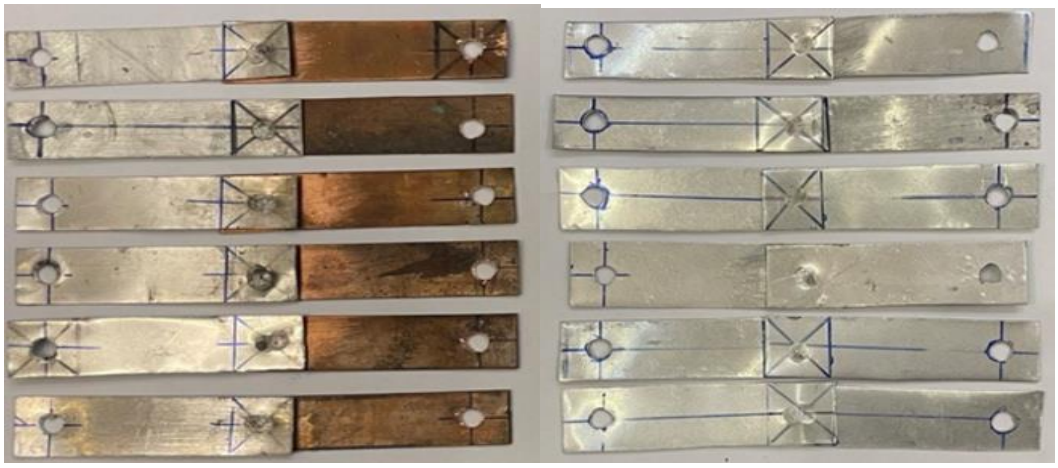

a)

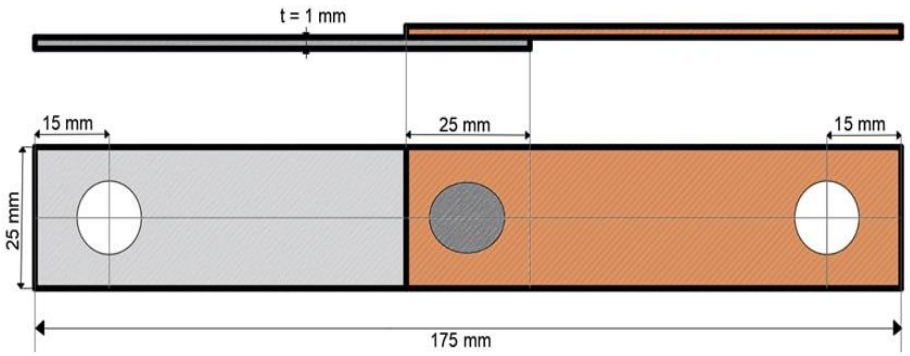

b)

Figure 9. a) RSW specimens b) RSW specimen dimensions for fatigue test

As mentioned before, the maximum applied load was determined by calibrating the load cell. Then, the specimen ends are securely connected between the jaws of the testing machine to ensure a strong and stable fixation. Additionally, the straightness of the specimen is carefully inspected, in a vertical orientation, to prevent any potential bending or side shearing issues during the testing procedure.

Once these preparatory steps were completed, the testing machine was set in motion to carry out the test cycles. Finally, run of the fatigue machine and observing the number of cycles with the crack length until the failure occurs; see Fig. 10. The results are meticulously recorded and saved in Excel sheet form for analysis and evaluation.

The fatigue test was done with the stress ratio, R = 0.1. The cyclic load was started at 60 % of the maximum tensile-shear load and decreased step by step. The ratio of every two adjacent loads ranged from 1 to 1.5, as mentioned in Ref. [48]. A ring made from brass with a lubricated container (handle greased) was used to decrease the friction caused by the cyclic load. The rotation motor and all of the device's components were installed on a thick and heavy steel base, in addition to rubber bases to minimize the vibration. The inner surface of the clamps is grooved to ensure that the sample does not slide. Fatigue tests were repeated by using two or three samples for each stress level. If the fatigue life difference between the two samples at the same load level was greater than 10 %, the test is repeated, see Fig. 11.

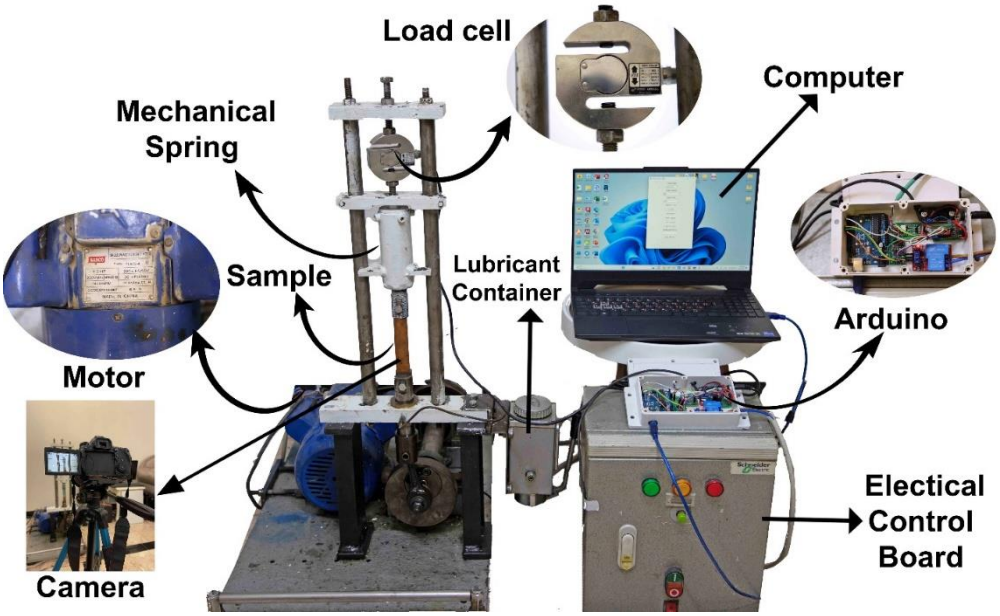

Figure 10. Fatigue test rig

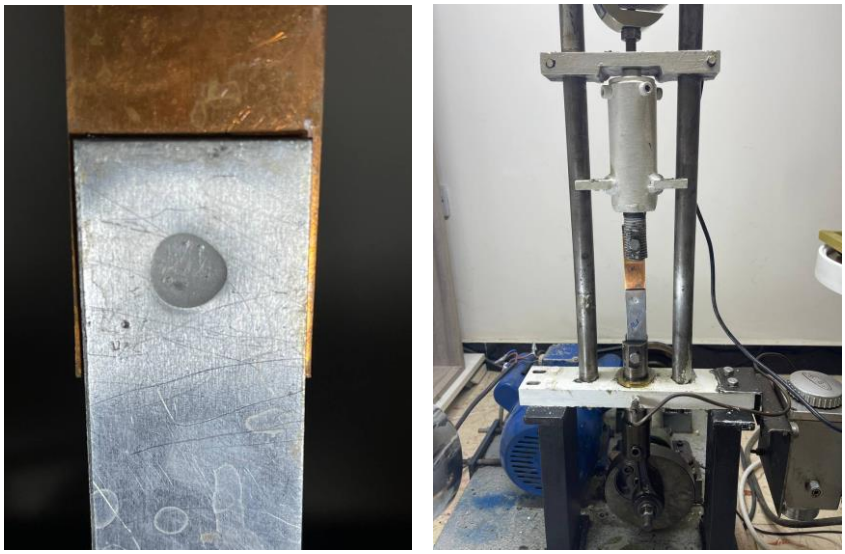

Figure 11. Specimen gripped in fatigue test

2.1.6. Crack Propagation

The RSW specimens were examined under the cyclic loading conditions to understand the failure modes and fatigue crack propagation of RSWs for similar and dissimilar joints, based on the fracture mechanics' approach. The tiny crack may exist initially, which gradually evolves into a crack and continues to grow under the cyclic loading to grow until it reaches a critical size. This is known as fatigue crack growth. As the stress range changes, the rate of crack propagation changes as well. Since the higher stress ranges result in more rapid crack growth, while the lower stress ranges lead to slower crack propagation (Fig. 12) [49]. The fatigue test, the measurement of crack length calculated by using a high-accuracy digital camera (Nikon Coolpix B 700), and the data were transformed in order to determine the length of the crack using the image processing software (ImageJ) on a computer; see Fig. 13. During the fatigue test and crack propagation, the number of cycles is measured for each crack length, which was determined by ImageJ.

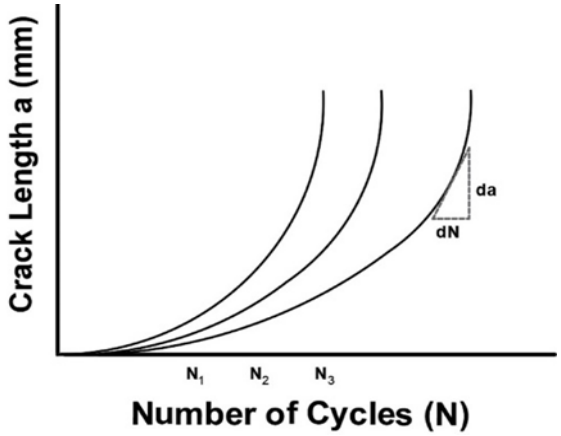

Figure 12. Number of cycle and crack length [49]

The Paris law (Eq. 1) describes the propagation of fatigue cracks in materials that are subjected to cyclic loading [50]. This equation is essential in understanding the crack growth rate over time, particularly in engineering applications where materials are subjected to cyclic stress, such as in structural elements, aircraft components, or mechanical parts [9], [51].

$$\frac{da}{dN} = C\,\Delta K^{m} \quad (1)$$

where a is the crack length (mm), N the number of cycles; C and m are the material coefficients; ΔK (SIF) is the stress intensity factor increment [52]; $\frac{da}{dN}$ is the crack growth rate and can be calculated for each increment (Δa), as follows:

$$\frac{da}{dN})_i = \frac{a_{i+1}-a_i}{N_{i+1}-N_i} \quad (i = 1, 2, 3) \quad (2)$$

In this work, the crack length at each number of cycles was determined. Crack lengths were calculated experimentally for each number of cycles during the fatigue test. Additionally, Finite Element (FE) numerical models validated the crack length and number of cycles from experiments.

2.2. Simulation Work

2.2.1. Finite Element Models

Several numerical simulation methods are used to investigate crack initiation and fatigue life based on the finite element method [53], [54], [55], [56]. ABAQUS-FE-based simulator was used to model the RSW specimens and evaluate their fracture toughness [57]. Finite Element (FE) software was used to determine the crack propagation and stress intensity factor (SIF) in similar and dissimilar SW joints based, on the linear elastic fracture mechanics approach (LEFM) [54]. Many steps must be completed to obtain the required results, including creating a 3D model, meshing, boundary conditions, and assigning material properties to run the RSW model. The model for RSW has been subdivided into the specific area that represents spot welding. This typically involves creating a circular region representing the nugget zone; see Fig. 14.

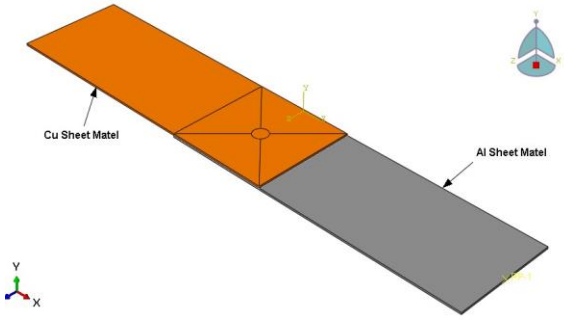

Figure 14. RSW-FE model

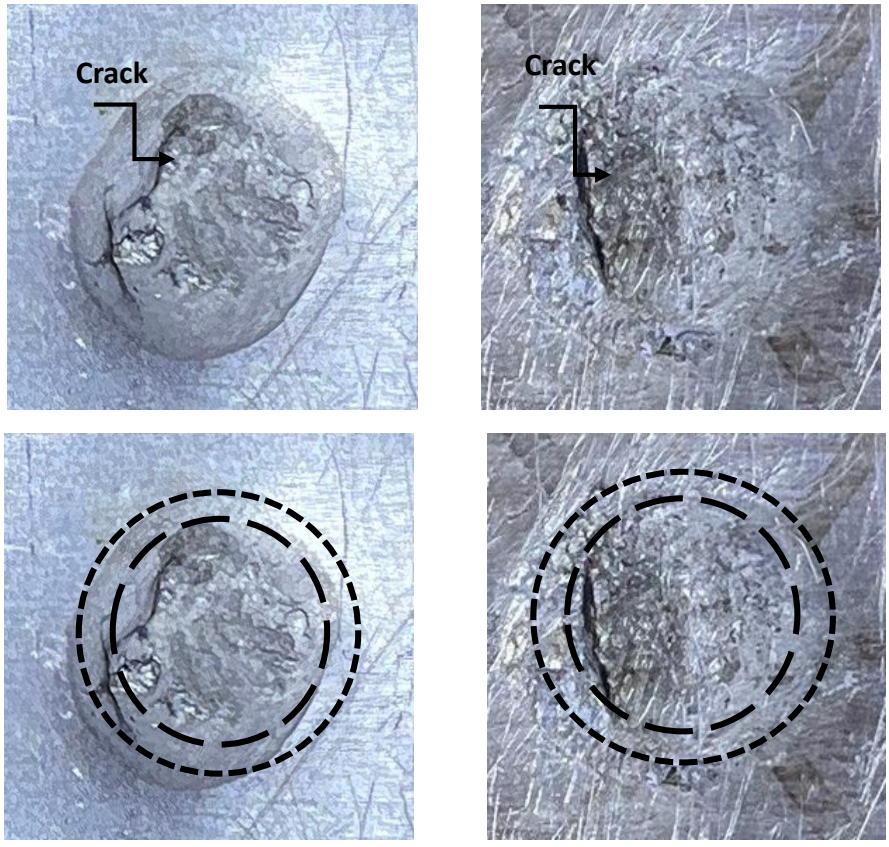

Figure 13. Crack propagation in dissimilar RSW joints, with the outer lines representing the heat-affected zone (HAZ) and the inner lines indicating the fusion zone (FZ)

The Linear Elastic Fracture Mechanics Approach (LEFM) has been applied to assess the crack propagation and stress intensity factor (SIF) calculations by utilizing advanced ABAQUS features. This FE-model can be used to provide a comprehensive understanding of fracture mechanics under cyclic loading conditions. To determine the SIF for welded specimens, the LEFM approach, which assumes the existence of an identified crack, has been used [58]. Von Mises stress is an important factor in RSW. It can be used to predict the stress concentration and load-bearing capacity of the welded joints. The maximum stress is found around the weld nugget areas [59]. Nevertheless, the crack location was validated by the tensile and fatigue tests as well. The initial crack is located at the maximum stress, a_i= 0.1 mm; see Fig. 15.

In ABAQUS, the meshing process involves discretizing a 3D model into element for analysis. Defining the element size for the mesh is very important. The work piece was meshed with 3D linear hexahedral elements of the C3D8R type; see Fig. 16a [60]. Those elements are commonly employed in FEA for their suitability for capturing the complex geometric shapes and structural behavior. The meshing strategy employed in this study involved a deliberate refinement of element size within the welding region, specifically the nugget zone, while gradually transitioning coarser elements in the surrounding areas; see Fig. 16b.

The accurate number of elements needed to mesh the plate was determined by the mesh convergence test. To prevent the outcomes of an analysis from being impacted by changing the size of the mesh, the mesh convergence test refers to the smallest elements that are suitable for the model [61], [62]. The effect of meshes and elements on the stress was examined; see Table 7. Therefore, the mesh is composed of a total number of 25784 nodes, and a total number of 21160 elements. The welding zone has the finer (and most crucial) region of the meshing; see Fig. 17.

Table 7. Mesh convergence effect

Elements Nr.	Max. Mises Stress (MPa)
8777	**8.5×10^7**
10520	**1.1×10^8**
15780	**5.42×10^8**
21160	**6.1×10^8**

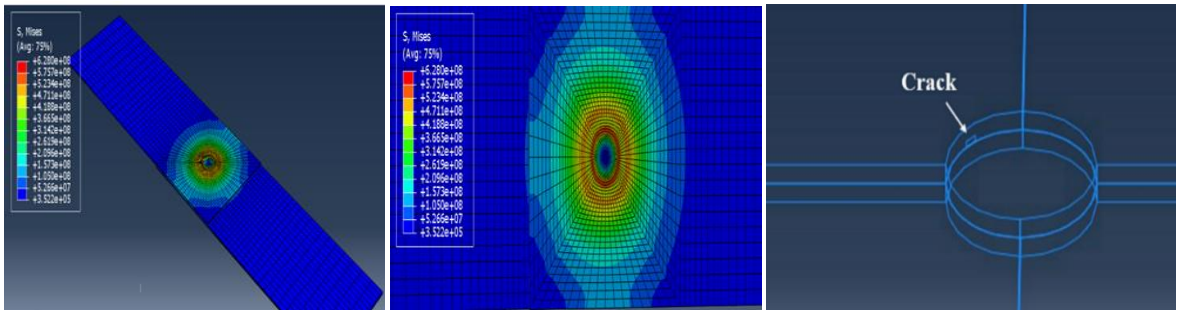

Figure 15. Von Mises stresses and initial crack in weld nugget, ABAQUS

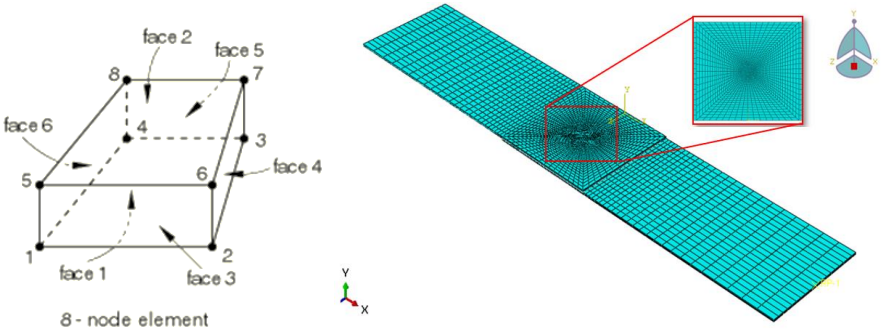

Figure 16. a) 3D Element 8-node type C3D8R; b) Mesh generation for RSW

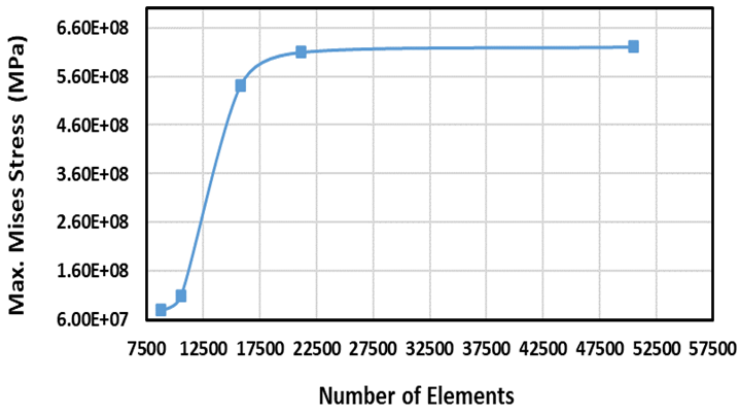

Figure 17. Meshes effect on the stresses of RSW joints

To execute an accurate simulation, input conditions for similar and dissimilar metals, such as optimum welding parameters and material properties (e.g., the elastic modulus, yield strength, and Poisson's ratio), were defined, as shown in Tables 3, 4, 5, and 6. Additionally, appropriate boundary conditions should be applied to replicate the actual loading conditions experienced by the welded joint. Then, the loading conditions are applied to simulate the tensile shear test. This typically involves defining a force boundary condition on one side of the joint while fixing the opposite side; see Fig. 18. The post-processing results, such as stress, SIF, crack propagation, and deformation, are then predicted.

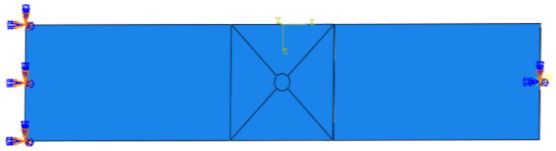

Figure 18. Boundary condition of RSW specimens

3. Results and Discussion

3.1. Tensile Shear Test

The strength of the overlapping resistance spot welded (RSW) joints was assessed using tensile shear tests. The results have been compared with available literature for other metals to demonstrate the validity of the current model and experiments. Table 8 shows the experimental results of similar (Al-Al) and dissimilar (Cu-Al) joint as compared to literature.

Table 8: Tensile shear strength (ST) for similar and dissimilar RSW joints, t=1 mm

Joints	Current Exp., ST (N)	ST (N)	FE-ST (N)
Cu-Al 1050	690	680 [63]	842
Al-Al (1050)	780	750 [64]	912
Al 6061-Steel	-	4600 [46]	5120
Al 5052-Steel	-	6200 [46]	6329

Figure 19 shows the validation of the simulated tensile shear force with forces obtained experimentally and from the literature review. The weld strength and differences (assuming differences between simulated results and validation results) can also occur due to parameter setup in the FE analysis, for example, mesh type and size [65].

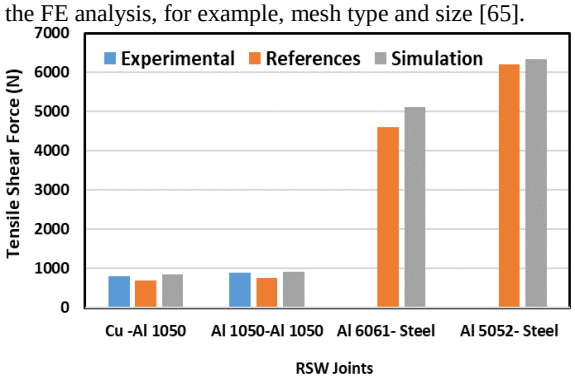

Figure 19. Tensile shear force for similar and dissimilar RSW joint as compared to Refs [46], [63], [64]

The dissimilar RSW may be chosen for its specific properties, even if joint strength is not necessarily being improved, as it can offer other benefits, such as electrical conductivity. The specimens for the spot after the tensile shear test failed in full pullout failure mode [66]. Traditionally, this mode occurs, meaning the weld has sufficient strength.

3.2. Fatigue Test

Spot welds have different zones of different microstructures, and hence, they are very critical to study for their fatigue failure [67], [68]. Fatigue life prediction for the RSW joints included the number of cycles and applied loads (P-N) curves. In addition, the number of cycles and crack length (a-N) curves are presented.

3.2.1. Fatigue Loads and Number of Cycle (P-N Curve)

The P-N curve test involves crack fatigue applied loads and number of cycles to failure; see Fig. 20.

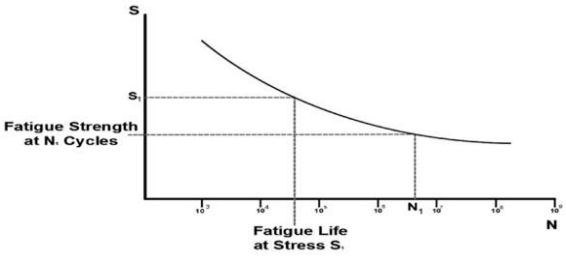

Figure 20. The P-N curve [69]

The fatigue test at R = 0.1, and frequency 10 Hz was carried out. The applied fatigue loads depend on the tensile shear force. It was taken at 10 %, 20 %, 30 %, 40 %, 50 %, and 60 % of tensile shear force. The experimental and numerical results of fatigue life of Al-Al joint are shown in Table 9. Figure 21 shows the fatigue life of similar RSW 1050 Al.

Table 9: Numerical and experimental fatigue life results of Al-Al SW joint at fatigue load equal to 10%, 20%, 30%, 40%, 50%, and 60% of tensile shear force

Max. Applied Load (kN)	Fatigue Life (Cycle)		Error %
	Exp.	FE-ABAQUS	
0.078	7122	8540	16.6
0.156	5356	6625	19.2
0.234	3130	3790	17.4
0.312	1140	1289	11.6
0.390	892	988	9.7
0.468	428	462	7.3

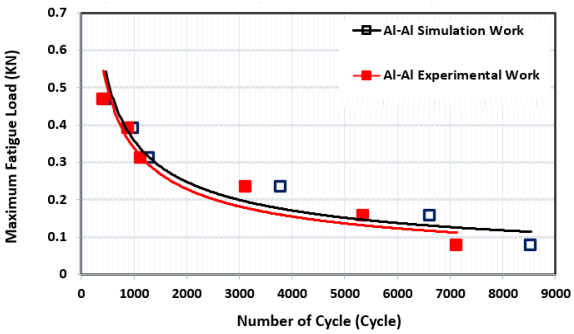

Figure 21. The P-N curve for 1050-Al RSW joint with applied fatigue loads at 10 %, 20 %, 30 %, 40 %, 50 %, and 60 % of tensile shear force

FE models have been validated with results from Ref. [70] for a similar joint of Al-Al only (see Table 10). Because, to the author's knowledge, there are no results about Al-Cu spot weld fatigue.

Table 10: Numerical fatigue life results of Al-Al RSW joint compared to Ref. [70]

Max. Applied Load (kN)	Fatigue Life (Cycle)		Error %
	Ref. [70]	FE-ABAQUS	
1.646	20	24	16.7
1.373	40	48	16.7
1.177	53	61	13.1
0.746	100	111	9.9
0.673	109	117	6.8
0.530	202	215	6
0.314	500	529	5.5

Figure 22 shows the 1050 aluminum RSW joining fatigue life simulation work and from the previous study [70]. At the same conditions as the ABAQUS simulation, the 1050 aluminum joining at the maximum applied load (1.646, 1.373, 1.177, 0.746, 0.673, 0.530, and 0.314 kN).

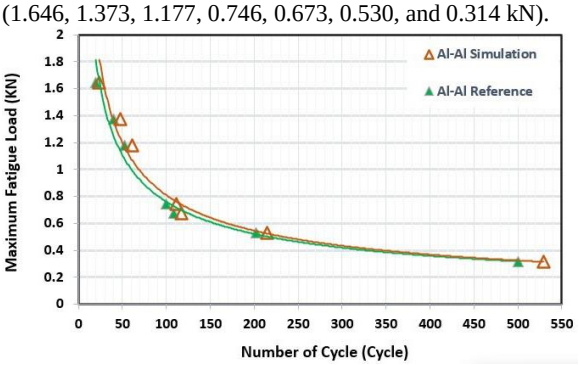

Figure 22. The P-N curve for 1050 aluminum joint; as compared to Ref. [70], t= 1mm

For dissimilar joints Al-Cu, a tensile shear force of 690 N. The sheet thickness was 1 mm. Fatigue life for such joints is shown in Table 11. The schematic results of Table 11 are presented in Fig. 23.

Table 11: Numerical and experimental fatigue life of Al-Cu RSW joint at fatigue load 10 %, 20 %, 30 %, 40 %, 50 %, and 60 % of tensile shear force

Max. Applied Load (kN)	Fatigue Life (Cycle)		Error %
	Exp.	FE-ABAQUS	
0.069	7001	8017	12.7
0.138	5199	6210	16.3
0.207	3001	3720	19.3
0.276	1022	1185	13.8
0.345	788	892	11.7
0.414	402	501	19.8

The fatigue behavior of RSWs can be classified into two categories; low cycle fatigue LCF and high-cycle fatigue HCF (Fig. 24). LCF occurs when the applied load is high enough to cause the plastic deformation in the material, leading to crack initiation and propagation. The fatigue crack initiation in LCF primarily occurs in the base material. The crack propagation occurs in the HAZ or the region close to the FZ [70]. In this work, HCF was predominant, because the applied load was below the yield strength of the spot welded joints.

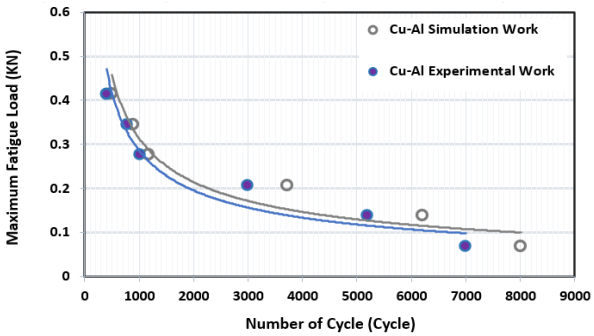

Figure 23. Experimental and numerical P-N curve for Cu-Al RSW joint with applied fatigue loads 10 %, 20 %, 30 %, 40 %, 50 %, and 60 % of tensile shear force

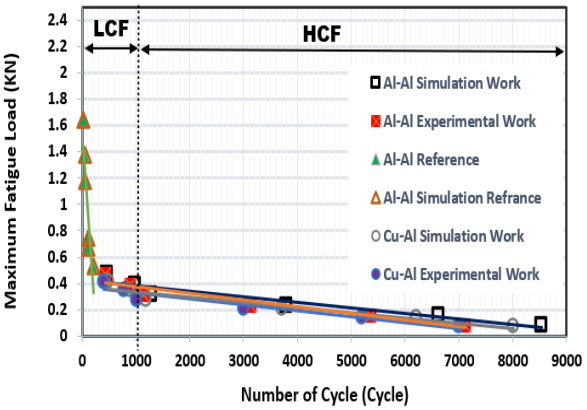

Figure 24. The P-N curve for Al-Al and Cu-Al RSW joints experimental and simulation work at applied force 10 %, 20 %, 30 %, 40 %, 50 %, and 60 % of tensile shear, Ref. [70] at LCF at the applied load (1.646, 1.373, 1.177, 0.746, 0.673, 0.530, and 0.314) kN

The similar Al-Al RSW joints have a longer fatigue life than the dissimilar Cu-Al RSW joints. Actually, this behavior agrees with the results of the tensile test [2], because the joining of Al and Cu has some differences in such techniques, such as the differences in mechanical and physical properties. Hence, a non-uniform weld nugget will be produced on each side. Antisymmetric nugget formation decreases the fatigue strength of the welded sheet combination.

3.2.2. Crack Length and Number of Cycles, a- N Curve

The crack length and the number of cycles in RSW are important factors that can affect the mechanical performance. The length of the cracks influences the fatigue life of the welded joint. Longer cracks tend to reduce the fatigue life of the joint, as they act as stress concentrators and can propagate more easily under cyclic loading conditions [71]. As mentioned before, the FE-fatigue analysis was carried out for sheet thickness of 1 mm with maximum applied loads, which represent 60 % of tensile shear (414) N and (468) N for the Al-Al and Al-Cu RSW joints, respectively. Hence, the crack length (a) was calculated experimentally using the ImageJ program; see Fig. 25. The shape of the crack in samples is usually clearly visible. It contains simple granular zigzags, as verified with Ref. [72].

The fatigue crack propagation of RSWs can be classified into two categories: LCF and HCF. The LCF occurs when the applied load is high enough to cause plastic deformation in the material, leading to crack initiation and propagation

from the base material. This crack path may be attributed to a biaxial stress distribution effect around the weld nugget [73]. The HCF (more than 10^3 cycles), in the case of current work, occurs when the applied load is below the yield strength of the material. Hence, crack propagation occurs in the HAZ, or FZ. The results agree with Ref. [74]; see Fig. 26.

Table 12 and Fig. 27 display the results for the crack length and number of cycles observed in both similar Al-Al joints and dissimilar Al-Cu joints.

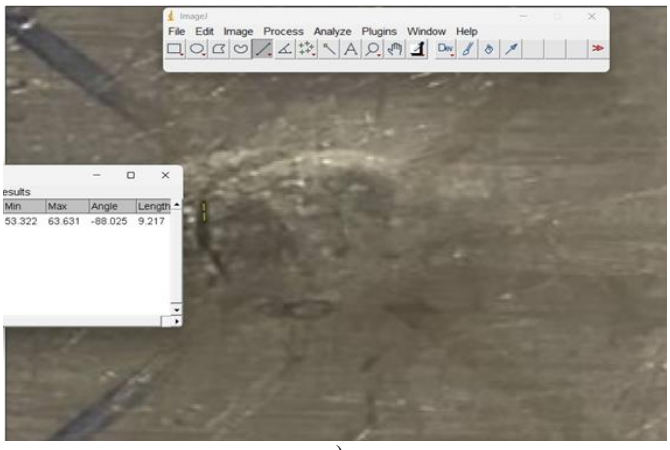

a)

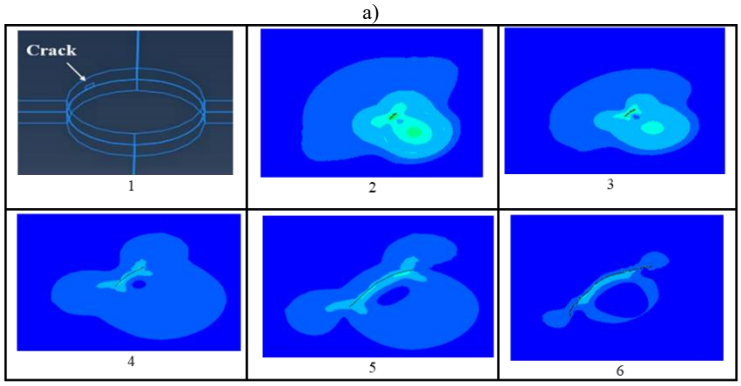

b)

Figure 25. Crack length calculation, a) Experimental work, b) FE simulation

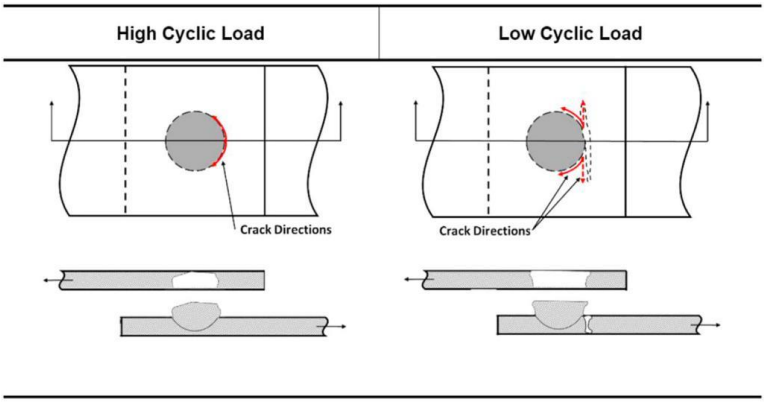

Figure 26. The LCF and HCF effects on the crack propagation behavior [74]

Table 12. Crack length and number of cycles at maximum applied loads 414 N and 468 N for the Al-Al and Al-Cu RSW joints

Experimental				Simulation			
Al-Cu Joint		Al-Al Joint		Al-Cu Joint		Al-Al Joint	
N (Cycle)	a (mm)	N (Cycle)	a (mm)	N (Cycle)	a (mm)	N (Cycle)	a (mm)
6780	1.2	6845	1.31	6888	1.31	6950	1.51
6820	1.6	6890	1.87	6970	1.9	7010	1.89
6911	2.4	6996	2.68	7010	2.42	7121	2.79
6955	2.91	7043	3.1	7082	3.21	7195	3.32
6979	3.12	7065	3.4	7099	3.3	7241	3.72
7001	3.36	7122	3.9	7110	3.41	7278	3.952

3.2.3. C and m Coefficients Determination

By conducting fatigue tests on the material, the crack growth rates (Δa/ΔN) under various stress levels and loading conditions can be measured. Hence, to determine the C and m coefficients, the following steps have been carried out:

1. Conducting fatigue tests to measure the crack growth rates.
2. Measuring the crack lengths at different intervals or cycles during the fatigue tests. This data provides the crack length (a) as a function of the number of cycles (N).
3. Calculating the SIF (K) for each crack length and load starts at 60 % of the tensile shear stress and decreases gradually for Al-Cu joints and Al-Al joints; see Table 13.
4. Calculate the crack growth rate (da/dN) by applying Eq. 2; see Table 14.

Figure 28 shows the crack growth rate against the stress intensity factor, KI. The crack growth rate of the similar RSW joint is lower than that of the dissimilar RSW joint because similar RSW joints have higher fracture toughness, requiring more cycles to reach the failure stage. Dissimilar RSW joints exhibit a faster crack growth rate compared to similar joints due to differences in material properties, metallurgical compatibility issues, and varying thermal behaviors. Hence, the crack initiation and propagation rates are increased for dissimilar joints, as seen in Fig. 28. By taking the logarithmic values of KI and da/dN, this data is plotted. The best fitting line represents the equations that determine the values of C and m [75]; refer to Fig. 29.

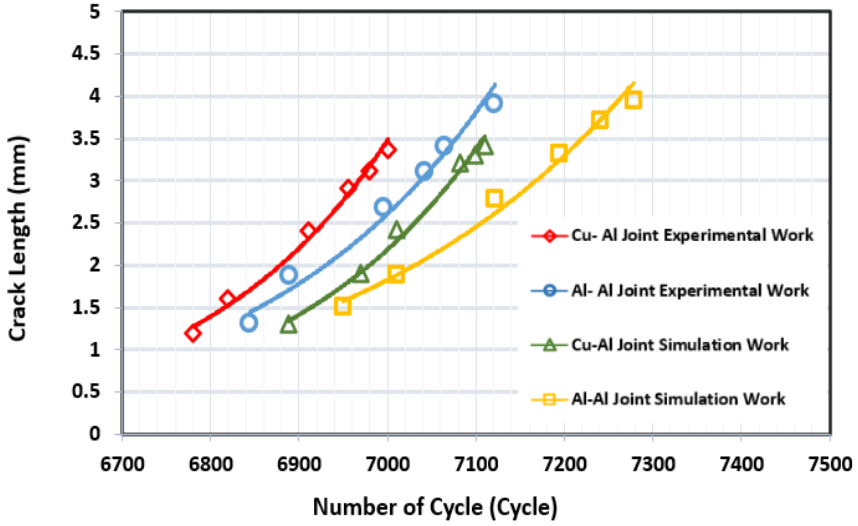

Figure 27. Crack Length and number of cycles; maximum applied loads 414 N, and 468 N for the Al-Al and Al-Cu RSW joints, respectively

Table 13. The SIF and number of cycles for RSW Joint by simulation at fatigue load 60 % of the maximum tensile shear load for Al-Cu and Al-Al joints

Al-Cu Joint			Al-Al Joint		
Max. Applied Load (kN)	KI (MPa √m)	N (Cycle)	Max. Applied Load (N)	KI (MPa √m)	N (Cycle)
0.069	0.021	7001	0.078	0.0121	7122
0.138	0.031	5544	0.156	0.0222	5485
0.207	0.0441	3050	0.234	0.033	3540
0.276	0.057	2850	0.312	0.0432	2712
0.345	0.068	2041	0.390	0.0564	2150
0.414	0.084	790	0.468	0.0691	867

Table 14. The SIF and crack length for RSW Joint by simulation

Al-Cu Joint				Al-Al Joint			
Max. Applied Load (N)	N (Cycle)	a (mm)	da/dN mm/Cycle	Max. Applied Load (N)	N (Cycle)	a (mm)	da/dN mm/Cycle
0.069	7001	3.36	0.000164722	0.078	7122	3.9	0.000305437
0.138	5544	3.12	0.0000842021	0.156	5485	3.4	0.000154242
0.207	3050	2.91	0.00255	0.234	3540	3.1	0.000507246
0.276	2850	2.4	0.000988875	0.312	2712	2.68	0.001797153
0.345	2041	1.6	0.000319744	0.390	2150	1.67	0.000280592
0.414	790	1.2	0.001518987	0.468	867	1.31	0.001510957

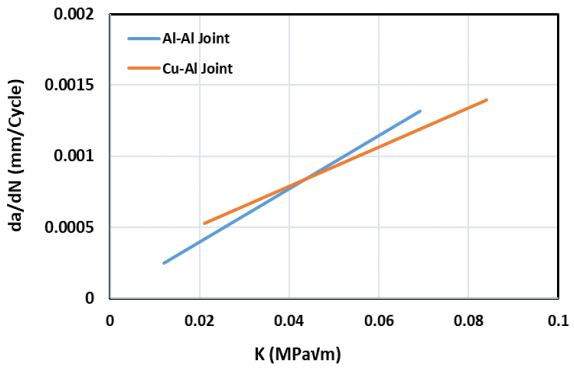

Figure 28. The Crack growth rate and SIF

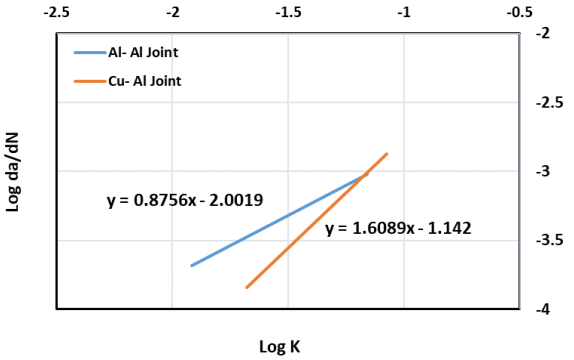

Figure 29. The Crack growth rate and SIF

The material coefficients of the spot-welded similar and dissimilar sheet joint are obtained from Fig. 29 as follows:

m = 1.6, and C = $10^{-1.142}$ for Cu-Al RSW joint

m = 0.87, and C = $10^{-2.0019}$ for Al-Al RSW joint

The of crack growth rate equation can be written as:

$da/dN = 10^{-1.142} \Delta K^{1.6}$ for Cu-Al RSW joint

$da/dN = 10^{-2.0019} \Delta K^{0.87}$ for Al-Al RSW joint

4. Conclusions

In this study, experimental and numerical methods were investigated to evaluate the fatigue strength of resistance spot welded (RSW) joints for aluminum 1050 and copper sheets. A fatigue tensile test rig was established to apply axial fatigue loads to RSW samples. The conclusions of this study are as follows:

1. The proposed model by ABAQUS was verified by comparing it to the experimental tensile and fatigue tests, to determine the fatigue life. In numerical simulations, the mesh density, element type, and convergence criteria can influence the accuracy of fatigue results. Coarser meshes or inadequate convergence can lead to less accurate results.
2. The high cycle fatigue (HCF) was applied, and the crack propagated around the spot-welding nugget, primarily within the fusion zone or along the boundary between the heat-affected zone (HAZ) and the fusion zone (FZ). Consequently, it extended around the nugget of the spot-welded structure as cyclic loading was continuously applied.
3. The mechanical properties of the RSW joint affect the fatigue life of these joints. Therefore, higher strength metals exhibit higher stress intensity factors (SIF) at the crack tip and shorter fatigue life. Hence, increasing the opening stress which increase the crack propagation rate.
4. The fatigue life of RSW joints is primarily influenced by the nugget diameters. These diameters were determined through experimental measurements and numerical simulations. Dissimilar joints exhibit a nonhomogeneous weld area in contrast to similar joints. Therefore, the dissimilar joints have a lower fatigue life, and a higher crack propagation rate.
5. The crack growth rate of the similar RSW joint is lower than that of the dissimilar RSW joint. That means the latter has a lower stress intensity factor and a higher fatigue life compared to dissimilar joints. Therefore, the similar RSW joint needs more time than the dissimilar RSW joint to reach the failure stage.
6. The crack growth rate equations for both similar and dissimilar joints were developed based on crack length and stress intensity factor (SIF). Therefore, the coefficients of the propagation rate equation were determined.

Nomenclature

Notation	Description	Units
RSW	Resistance Spot Welding	
Al-Cu	Aluminium–Copper Joint	
Cu-Cu	Copper–Copper Joint	
Al-Al	Aluminium–Aluminium Joint	
BM	Base Metal	
HAZ	Heat Affected Zone	
FZ	Fusion Zone	
K	Stress Intensity Factor (SIF)	MPa√m
a	Crack length	mm
C, m	Paris–Erdogan material coefficients	
D	Spot Weld or Nugget Diameter	mm
da /dN	Crack growth rate	mm/cycle
E	Modulus of elasticity	MPa
FEA	Finite Elements Analyses	
R	Load ratio	
S	Stress	MPa
N	Number of Cycle	cycles
ST	Tensile strength	N
t	Sheet Thickness	mm

References

[1] M. S. Fakhri, A. M. Al-Mukhtar, and I. A. Mahmood, "Comparative Study of the Mechanical Properties of Spot Welded Joints," *Mater. Sci. Forum*, vol. 1079, pp. 21–28, Dec. 2022, doi: 10.4028/p-488xsr.

[2] M. S. Fakhri, A. Al-Mukhtar, and I. A. Mahmood, "Effect Of Mechanical Deformation On The Electrical Conductivity Of Resistance Spot Welding Joints," *J. Appl. Sci. Eng. Taiwan*, vol. 27, no. 9, pp. 3095–3103, 2024, doi: 10.6180/jase. 202409_27(9).0007.

[3] M. Fakhri, I. Mahmood, and A. Al-Mukhtar, "The Electrical and Mechanical Aspects of Aluminum and Copper Resistance Spot Weld Joints," *Eng. Technol. J.*, vol. 0, no. 0, pp. 1–11, Dec. 2023, doi: 10.30684/etj.2023.143734.1606.

[4] M. Anastassiou, M. Babbit, and J. L. Lebrun, "Residual stresses and microstructure distribution in spot-welded steel sheets: Relation with fatigue behaviour," *Mater. Sci. Eng. A*, vol. 125, no. 2, pp. 141–156, 1990.

[5] L. CHELBI, F. HENTATI, and A. ZNAIDI, "Analysis of Fatigue Life and Crack Growth in Austenitic Stainless Steel AISI 304l.," *Jordan Journal of Mechanical and Industrial Engineering*, vol. 17, no. 4, 2023.

[6] K. Ni and S. Mahadevan, "Probabilistic fatigue crack growth analysis of spot-welded joints," *Fatigue Fract. Eng. Mater. Struct.*, vol. 27, no. 6, pp. 473–480, 2004.

[7] M. A. Maleque, M. S. Salit, M. A. Maleque, and M. S. Salit, "Mechanical failure of materials," *Mater. Sel. Des.*, pp. 17–38, 2013.

[8] J. A. Collins, *Failure of materials in mechanical design: analysis, prediction, prevention*. John Wiley & Sons, 1993.

[9] A. F. Liu, *Mechanics and mechanisms of fracture: an introduction*. ASM International, 2005.

[10] A. M. Al-Mukhtar, "Aircraft Fuselage Cracking and Simulation," *Procedia Struct. Integr.*, vol. 28, pp. 124–131, 2020, doi: 10.1016/j.prostr.2020.10.016.

[11] G. Totten, "Fatigue crack propagation," *Adv. Mater. Process.*, vol. 166, no. 5, pp. 39–42, 2008.

[12] H. Mao and S. Mahadevan, "Fatigue damage modelling of composite materials," *Compos. Struct.*, vol. 58, no. 4, pp. 405–410, 2002.

[13] O. Salomon, F. Rastellini, S. Oller, and E. Onate, "Fatigue prediction for composite materials and structures," presented at the Air vehicle technology: AVT-121. Symposium on the evaluation, control and prevention of high cycle fatigue, 2005.

[14] S. Donders, M. Brughmans, L. Hermans, and N. Tzannetakis, "The effect of spot weld failure on dynamic vehicle performance," *Sound Vib.*, vol. 39, no. 4, pp. 16–25, 2005.

[15] H. Mughrabi, "Microstructural mechanisms of cyclic deformation, fatigue crack initiation and early crack growth," *Philos. Trans. R. Soc. Math. Phys. Eng. Sci.*, vol. 373, no. 2038, p. 20140132, 2015.

[16] H. Gaul, G. Weber, and M. Rethmeier, "Influence of HAZ cracks on fatigue resistance of resistance spot welded joints made of advanced high strength steels," *Sci. Technol. Weld. Join.*, vol. 16, no. 5, pp. 440–445, 2011.

[17] R. W. Rathbun, D. K. Matlock, and J. G. Speer, "Fatigue behavior of spot welded high-strength sheet steels," MSc. Thesis, Trustees of the Colorado School of Mines, 2003.

[18] J. A. Davidson, "A review of the fatigue properties of spot-welded sheet steels," *SAE Trans.*, pp. 35–47, 1983.

[19] Y. P. Yang, S. S. Babu, F. Orth, and W. Peterson, "Integrated computational model to predict mechanical behaviour of spot weld," *Sci. Technol. Weld. Join.*, vol. 13, no. 3, pp. 232–239, Apr. 2008, doi: 10.1179/174329308X283901.

[20] Y. P. Yang, J. Gould, W. Peterson, F. Orth, P. Zelenak, and W. Al-Fakir, "Development of spot weld failure parameters for full vehicle crash modelling," *Sci. Technol. Weld. Join.*, vol. 18, no. 3, pp. 222–231, Apr. 2013, doi: 10.1179/1362171812Y.0000000082.

[21] D. Heidrich, F. Zhang, and X. Fang, "Fatigue strength of rivet resistance spot welding technique in comparison with self-piercing riveting for multi-material body-in-white structure," *J. Mater. Eng. Perform.*, vol. 30, no. 5, pp. 3806–3821, 2021.

[22] D. S. Sahota, R. Singh, R. Sharma, and H. Singh, "Study of effect of parameters on resistance spot weld of ASS316 material," *Mech. Confab*, vol. 2, no. 2, pp. 67–78, 2013.

[23] A. M. Al-Mukhtar, S. A. K. Al-Jumaili, and A. H. F. Al-Jlehawy, "Effect of Heat Treatments on 302 Austenitic Stainless Steel Spot Weld," *Adv. Eng. Forum*, vol. 29, pp. 19–25, Aug. 2018, doi: 10.4028/www.scientific.net/AEF.29.19.

[24] V. L. Acoff, R. G. Thompson, R. D. Griffin, and B. Radhakrishnan, "Effect of heat treatment on microstructure and microhardness of spot welds in Ti-26A1-11Nb," *Mater. Sci. Eng. A*, vol. 152, no. 1–2, pp. 304–309, May 1992, doi: 10.1016/0921-5093(92)90083-D.

[25] S. Aslanlar, a. Ogur, U. Ozsarac, E. Ilhan, and Z. Demir, "Effect of welding current on mechanical properties of galvanized chromided steel sheets in electrical resistance spot welding," *Mater. Des.*, vol. 28, no. 1, pp. 2–7, Jan. 2007, doi: 10.1016/j.matdes.2005.06.022.

[26] S. Aslanlar, A. Ogur, U. Ozsarac, and E. Ilhan, "Welding time effect on mechanical properties of automotive sheets in electrical resistance spot welding," *Mater. Des.*, vol. 29, no. 7, pp. 1427–1431, 2008.

[27] A. M. Al-Mukhtar and Q. Doos, "The Spot Weldability of Carbon Steel Sheet," *Adv. Mater. Sci. Eng.*, vol. 2013, pp. 1–6, 2013, doi: 10.1155/2013/146896.

[28] S. Dwivedi and S. Sharma, "Optimization of Resistance Spot Welding Process Parameters on Shear Tensile Strength of SAE 1010 steel sheets Joint using Box-Behnken Design.," *Jordan Journal of Mechanical and Industrial Engineering*, vol. 10, no. 2, 2016.

[29] J. R. Davis, Ed., *Tensile testing*, 2. ed. Materials Park, Ohio: ASM International, 2004.

[30] T. Wang, T. Zhu, J. Sun, R. Wu, and M. Zhang, "Influence of rolling directions on microstructure, mechanical properties and anisotropy of Mg-5Li-1Al-0.5Y alloy," *J. Magnes. Alloys*, vol. 3, no. 4, pp. 345–351, 2015, doi: 10.1016/j.jma.2015.11.001.

[31] D. Zhao, D. Ren, K. Zhao, S. Pan, and X. Guo, "Effect of welding parameters on tensile strength of ultrasonic spot welded joints of aluminum to steel – By experimentation and artificial neural network," *J. Manuf. Process.*, vol. 30, pp. 63–74, Dec. 2017, doi: 10.1016/j.jmapro.2017.08.009.

[32] T. V Christy, N. Murugan, and S. Kumar, "A comparative study on the microstructures and mechanical properties of Al 6061 alloy and the MMC Al 6061/TiB2/12p," *J. Miner. Mater. Charact. Eng.*, vol. 9, no. 1, pp. 57–65, 2010.

[33] Y. Li, L. Li, J. Nie, Y. Cao, Y. Zhao, and Y. Zhu, "Microstructural evolution and mechanical properties of a 5052 Al alloy with gradient structures," *J. Mater. Res.*, vol. 32, no. 23, pp. 4443–4451, 2017.

[34] S. Jitsukawa *et al.*, "Development of an extensive database of mechanical and physical properties for reduced-activation martensitic steel F82H," *J. Nucl. Mater.*, vol. 307, pp. 179–186, 2002.

[35] P. Kah, C. Vimalraj, J. Martikainen, and R. Suoranta, "Factors influencing Al-Cu weld properties by intermetallic compound formation," *Int. J. Mech. Mater. Eng.*, vol. 10, no. 1, 2015, doi: 10.1186/s40712-015-0037-8.

[36] İ. Ay, S. Çelik, and İ. Çelik, "Comparison of properities of friction and diffusion welded joints made between the aluminium and copper bars," *Balıkesir Üniversitesi Fen Bilim. Enstitüsü Derg.*, vol. 2, no. 1, pp. 88–102, 2000.

[37] M. A. Taha, R. A. Youness, and M. A. Ibrahim, "Evolution of the physical, mechanical and electrical properties of sic-reinforced Al 6061 composites prepared by stir cast method," *Biointerface Res Appl Chem*, vol. 11, pp. 8946–8956, 2021.

[38] E. B. Moustafa *et al.*, "Influence of friction stir process on the physical, microstructural, corrosive, and electrical properties of an Al–Mg alloy modified with Ti–B additives," *Materials*, vol. 15, no. 3, p. 835, 2022.

[39] H. Zhang and J. Senkara, *Resistance welding: fundamentals and applications*. CRC press, 2011.

[40] A. Ambroziak and M. Korzeniowski, "Using resistance spot welding for joining aluminium elements in automotive industry," *Arch. Civ. Mech. Eng.*, vol. 10, no. 1, pp. 5–13, 2010, doi: 10.1016/s1644-9665(12)60126-5.

[41] K. M. Daws, M. H. Al-saadi, and I. K. A. Al-naimi, "Investigation Parameters of Resistance Spot Welding For AA1050 Aluminum Alloy Sheets," *J. Eng.*, vol. 18, no. 10, pp. 1128–1141, 2012.

[42] K. Milkey, A. Samsudin, A. Dubey, and P. Kidd, "Comparison between Taguchi Method and Response Surface Methodology (RSM) in Modelling CO 2 Laser Machining.," *Jordan Journal of Mechanical and Industrial Engineering*, vol. 8, no. 1, 2014.

[43] T. Alsardia and L. Lovas, "Investigation of the Effect of the Surface Treatment and Lubrication During Repeated Tightening on the Nut Coefficient of a Bolted Joint Using the Taguchi Method," *JJMIE*, vol. 81, no. 1, 2024.

[44] U. Eşme, "Application of Taguchi Method for the Optimization of Resistance Spot Welding Process," *Arab. J. Sci. Eng. Springer Sci. Bus. Media BV*, vol. 34, 2009.

[45] A. Sahoo, S. Tripathy, and D. Tripathy, "Parametric Optimization of Pulse TIG Welding Process during Joining of Dissimilar Tensile Steels Used in Automotive Industries.," *Jordan Journal of Mechanical and Industrial Engineering*, vol. 16, no. 5, 2022.

[46] S. M. Manladan, F. Yusof, S. Ramesh, M. Fadzil, Z. Luo, and S. Ao, "A review on resistance spot welding of aluminum alloys," *Int. J. Adv. Manuf. Technol.*, vol. 90, no. 1–4, pp. 605–634, 2017, doi: 10.1007/s00170-016-9225-9.

[47] S. Khammass Hussein and O. Sabah Barrak, "Analysis and Optimization of Resistance Spot Welding Parameter of Dissimilar Metals Mild Steel and Aluminum Using Design of Experiment Method," *Eng TechJournal*, vol. 33, no. 8, 2015.

[48] H. Long, Y. Hu, and X. Jin, "Stress intensity factor solutions and fatigue estimation for dual phase and low-carbon steel spot weld," *Theor. Appl. Fract. Mech.*, vol. 96, pp. 408–417, 2018.

[49] E. J. Hearn, *Mechanics of Materials 2: The mechanics of elastic and plastic deformation of solids and structural materials*. Elsevier, 1997.

[50] A. Kheder, N. Jubeh, and E. Tahah, "Fatigue Properties under Constant Stress/Variable Stress Amplitude and Coaxing Effect of Acicular Ductile Iron and 42 CrMo4 Steel.," *Jordan Journal of Mechanical and Industrial Engineering*, vol. 5, no. 4, 2011.

[51] P. Paris and F. Erdogan, "A critical analysis of crack propagation laws," *J Basic Eng*, pp. 528–533, 1963, doi: org/10.1115/1.3656900.

[52] H. Eskandari, "Stress intensity factors for crack located at an arbitrary position in rotating FGM disks," *JJMIE*, vol. 8, no. 1, 2014.

[53] L. Jie, Z. Xin, H. Yuanjun, H. Bo, and G. Jingbo, "Numeral Analysis of Crack Initiation Life on Tunnel Boring Machine Cutter Seat.," *Jordan Journal of Mechanical and Industrial Engineering*, vol. 16, no. 5, 2022.

[54] A. M. Al-Mukhtar, S. Henkel, H. Biermann, and P. Hübner, "A finite element calculation of stress intensity factors of cruciform and butt welded joints for some geometrical parameters," *Jordan Journal of Mechanical and Industrial Engineering*, vol. 3, no. 4, pp. 236–245, 2009.

[55] E. Rezaei, M. Poursina, M. Rezaei, and A. Ariaei, "A new analytical approach for crack modeling in spur gears," *JJMIE*, vol. 13, no. 2, 2019.

[56] F. Zeqiri and B. Fejzaj, "Experimental Research and Mathematical Modeling of Parameters Affecting Cutting Tool Wear in Turning Process of Inconel 625," *JJMIE*, vol. 16, no. 5, pp. 787–792, 2022.

[57] "Abaqus," Dassault Systèmes. Accessed: Apr. 05, 2024. [Online]. Available: https://www.3ds.com/products/simulia/abaqus

[58] R. I. Stephens, A. Fatemi, R. R. Stephens, and H. O. Fuchs, *Metal fatigue in engineering*. John Wiley & Sons, 2000.

[59] D.-A. Wang and J. Pan, "A computational study of local stress intensity factor solutions for kinked cracks near spot welds in lap-shear specimens," *Int. J. Solids Struct.*, vol. 42, no. 24–25, pp. 6277–6298, 2005.

[60] S. Kalmykova, "Simulation of T-joints between RHS steel members with offset in Abaqus CAE," *Acta Polytech. CTU Proc.*, vol. 30, pp. 36–40, 2021.

[61] H. Abdulsalam, "Mesh sensitivity assessment on 2D and 3D elastic finite element analysis on a compact tension specimen geometry using ABAQUS/CAE software," in *IOP Conference Series: Earth and Environmental Science*, IOP Publishing, 2021, p. 12032.

[62] R. Beckmann, R. Mella, and M. R. Wenman, "Mesh and timestep sensitivity of fracture from thermal strains using peridynamics implemented in Abaqus," *Comput. Methods Appl. Mech. Eng.*, vol. 263, pp. 71–80, 2013.

[63] M. H. Sar, M. H. Ridha, I. M. Husain, and S. K. Hussein, "Influence of Welding Parameters of Resistance Spot Welding On Joining Aluminum with Copper," vol. 27, no. 2, pp. 217–225, 2022, doi: 10.2478/ijame-2022-0029.

[64] I. K. Al Naimi, M. H. Al Saadi, K. M. Daws, and N. Bay, "Influence of surface pretreatment in resistance spot welding of aluminum AA1050," *Prod. Manuf. Res.*, vol. 3, no. 1, pp. 185–200, 2015, doi: 10.1080/21693277.2015.1030795.

[65] I. M. Husain, M. L. Saad, O. S. Barrak, S. K. Hussain, and M. M. Hamzah, "Shear force analysis of Resistance Spot Welding of Similar and Dissimilar Material: copper and carbon steel," in *IOP Conference Series: Materials Science and Engineering*, IOP Publishing, 2021, p. 12055.

[66] A. Arumugam and A. Pramanik, "Review of Experimental and Finite Element Analyses of Spot Weld Failures in Automotive Metal Joints.," *Jordan Journal of Mechanical and Industrial Engineering*, vol. 14, no. 3, 2020.

[67] A. Pasarkar, A. Mane, N. Singh, A. Datarkar, and N. Raut, "A Review of fatigue behaviour of resistance spot welds preventers," *Res. Eng. Struct. Mater.*, 2022, doi: 10.17515/resm2022.509me0824tn.

[68] A. M. Al-Mukhtar, "Review of Resistance Spot Welding Sheets: Processes and Failure Mode," *Adv. Eng. Forum*, vol. 17, pp. 31–57, Jun. 2016, doi: 10.4028/www. scientific .net/AEF.17.31.

[69] C. Li, S. Wu, J. Zhang, L. Xie, and Y. Zhang, "Determination of the fatigue PSN curves–A critical review and improved backward statistical inference method," *Int. J. Fatigue*, vol. 139, p. 105789, 2020.

[70] M. K. Wahid, M. N. Muhammed Sufian, and M. S. Firdaus Hussin, "Effect of fatigue test on spot welded structural joint," *J. Teknol.*, vol. 79, no. 5–2, pp. 95–99, 2017, doi: 10.11113/jt.v79.11290.

[71] A. M. Al-Mukhtar, "Investigation of the Thickness Effect on the Fatigue Strength Calculation," *J. Fail. Anal. Prev.*, vol. 13, no. 1, pp. 63–71, Feb. 2013, doi: 10.1007/s11668-012-9629-2.

[72] N. Pan and S. D. Sheppard, "Stress intensity factors in spot welds," *Eng. Fract. Mech.*, vol. 70, no. 5, pp. 671–684, 2002, doi: https://doi.org/10.1016/S0013-7944(02)00076-0.

[73] A. M. Al-Mukhtar, "Mixed-Mode Crack Propagation in Cruciform Joint using Franc2D," *J. Fail. Anal. Prev.*, pp. 1–7, 2016, doi: 10.1007/s11668-016-0094-1.

[74] G. G. Yapici and I. J. Ibrahim, "On the fatigue and fracture behavior of keyhole-free friction stir spot welded joints in an aluminum alloy," *J. Mater. Res. Technol.*, vol. 11, pp. 40–49, 2021.

[75] M. Vural, a. Akkuş, and B. Eryürek, "Effect of welding nugget diameter on the fatigue strength of the resistance spot welded joints of different steel sheets," *J. Mater. Process. Technol.*, vol. 176, no. 1–3, pp. 127–132, Jun. 2006, doi: 10.1016/j.jmatprotec.2006.02.026.